Preparation, Characterization, and Performance of Fe−ZSM-5 Catalysts

ARTICLE *in* THE JOURNAL OF PHYSICAL CHEMISTRY B · JULY 1999

Impact Factor: 3.3 · DOI: 10.1021/jp990978m

2 AUTHORS:

Rw Joyner
Nottingham Trent University
143 PUBLICATIONS **3,296** CITATIONS
SEE PROFILE

Michael Stockenhuber
University of Newcastle
65 PUBLICATIONS **1,051** CITATIONS
SEE PROFILE

Preparation, Characterization, and Performance of Fe−ZSM-5 Catalysts

Richard Joyner* and Michael Stockenhuber†

Catalysis Research Laboratory, Department of Chemistry and Physics, Nottingham Trent University, Clifton Lane, Nottingham NG11 8NS, U.K.

Received: March 22, 1999; In Final Form: May 11, 1999

A number of iron−ZSM-5 catalysts have been prepared and characterized by X-ray absorption spectroscopy using fluorescence detection, electron spectroscopy, temperature-programmed reduction, infrared spectroscopy, and electron microscopy. Iron has been introduced by aqueous exchange, by a novel method recently proposed by Feng and Hall (*Catal. Lett.* **1996**, *41*, 45), by exchange from a rigorously dried methanolic solution accompanied by agitation with ultrasound, and by a method intended to promote solid-state exchange. The degree of interaction with the zeolite framework has been probed by examining the effect on the zeolite proton OH band in the infrared spectrum. Less than 30% of the protons were exchanged from aqueous solution, but almost 80% exchange was achieved using ultrasound, as well as by the method reported by Feng and Hall (FH). Initially, both methods exhibited mainly isolated metal ions; however, calcination of the samples prepared according to FH exhibited rather large oxide clusters. After aqueous exchange and activation, most of the iron is present in the form of small oxygen-containing nanoclusters within the zeolite matrix, with EXAFS measurements indicating an average composition of Fe_4O_4, although electron microscopy identifies some larger particles at the external surface of the zeolite. Depending on the preparation methods, isolated cationic species within the zeolite matrix were also found. The small Fe_4O_4 type clusters cannot be reduced to the metallic state, even by hydrogen at 1100 K, although interconversion between Fe(II) and Fe(III) is facile. When the zeolite was exposed to nitric oxide, stretching vibrations corresponding to adsorption on the different iron species present could be identified by infrared spectroscopy. It is proposed that the ultrastable iron−oxygen nanoclusters have structures similar either to the iron−sulfur compounds ferredoxin II of desulfovibrio Gigas or to the cubanes of high-potential iron protein (HIPIP). Reactivity of these Fe−ZSM-5 materials in the selective catalytic reduction of NO_x by propene in oxygen/helium differs significantly, depending irreversibly on whether they are initially activated in oxygen or in an inert atmosphere. Correlations between catalytic activity and the infrared spectroscopy results for adsorbed NO indicate that the nanoclusters are more active (per iron atom) in the SCR reaction than the isolated cations.

1. Introduction

Although iron-exchanged zeolites were first prepared and characterized in the late 1960s,[1,2] these materials have attracted considerable catalytic interest only quite recently. It has been found that ion-exchanged Fe−ZSM-5 can decompose nitrous oxide[3,4] and also act as a redox catalyst for the oxidation of benzene to phenol[5] and the selective oxidation of methane.[5a] In a survey of zeolite ion-exchanged with different metals, iron−mordenite has been reported to be highly active for the selective catalytic reduction of nitrogen oxides under lean burn conditions, (the so-called selective catalytic reduction (SCR) reaction).[6] Recently, Fe−ZSM-5 has attracted interest in SCR, since the report by Feng and Hall (hereafter referred to as FH) that catalysts prepared in an unusual way may show stable, high performance in the presence of both water and sulfur dioxide.[7] However, in light of the importance of iron as an ammonia synthesis catalyst, as a redox catalyst for water gas shift, and also in biological systems, it is perhaps surprising that catalysis over Fe−ZSM-5 zeolites has attracted much less interest than, for example, Cu−ZSM-5. Also, compared to Cu−ZSM-5, little has been published on the characterization of these materials. X-ray absorption spectroscopy is a technique of choice,[8] but because of its relatively low absorption cross section, iron at low concentration is difficult to investigate. Although a few studies have been made of Fe−silicalite,[9−11] the first paper on ion-exchanged Fe−ZSM-5 appeared only recently.[12] However, the authors were able to interpret only the near-edge XANES region of the spectrum because of the poor signal-to-noise ratio in transmission mode measurements. We have overcome this difficulty by measuring in the fluorescence mode.

Unlike other transition metal exchanged zeolites, in particular copper, there is little information available on overexchanged or even highly exchanged iron-containing samples. With the exceptions of solid-state exchanged materials[13] and FH,[7,14] who report overexchange by excluding the exchange solution from the zeolite, the maximum exchange of the charge-balancing cation is approximately 70%.[2] Recently, Hall and Dumesic reported low reproducibility of catalysts prepared from different initial zeolite sources, as well as an increased catalytic activity of materials when the catalysts is first activated in the absence of oxygen.[15] Activation procedures are found to determine catalytic activity as well as NO adsorption capacities. We will discuss possible reasons for the low exchange capacity for iron in zeolites, as well as different models for the state of the iron in the zeolite. We will also show that considerable differences exist in the type of iron species formed, depending subtly on the initial

* Corresponding author. Phone: 44-115-948-6837. Fax: 44-115-948-6838: E-mail: richard.joyner@ntu.ac.uk.
† Phone/fax: 44-115-948-6694. E-mail: michael.stockenhuber@ntu.ac.uk.

10.1021/jp990978m CCC: $18.00
Published on Web 00/00/0000 PAGE EST: 13.3

TABLE 1: Basic Information on the Materials Studied

catalyst designation (see text)	iron content (wt %)	iron content (mol g^{-1})	aluminium content (mol g^{-1})	acidic protons exchanged[a] (%)	$Fe/H^+_{exchanged}$
Fe-ZSM-5	0.71	1.27×10^{-4}	4.50×10^{-4}	27.0	1.04
Fe-ZSM-5-50%	0.36	6.48×10^{-5}	4.50×10^{-4}	15.5	0.92
Fe-ZSM-5 (MeOH)	0.75	1.34×10^{-4}	4.94×10^{-4}	76.5	0.35
Fe-ZSM-5 B (FH)	1.5	2.15×10^{-4}	4.94×10^{-4}	73.8	0.59
Fe-ZSM-5 C ($FeCl_2$SS)	2.91	5.21×10^{-4}	4.50×10^{-4}	35.3	2.99
Fe-ZSM-5 ($FeCO_3$, SS)	2.65	4.75×10^{-4}	4.50×10^{-4}	35.8	3.23

[a] Determined by infrared spectroscopy; see text.

formation conditions of the exchanged material. Last, we briefly report the catalytic activity of a number of Fe−ZSM-5 materials in the SCR reaction, using propene as the reductant.

A number of characterization methods have been applied that are capable of revealing most of the interesting and important aspects of these materials. The interaction of the iron species with the Brønsted sites of the zeolite has been probed using infrared spectroscopy, and the spatial distribution of iron species through the zeolite examined using both high-resolution transmission microscopy coupled with energy dispersive analysis of X-rays (EDAX) elemental analysis, X-ray photoelectron spectroscopy, and extended X-ray absorption fine structure spectroscopy (EXAFS). The redox behavior and oxidation state of iron in the materials has been probed using temperature-programmed reduction (TPR), X-ray absorption near-edge spectroscopy (XANES), and also infrared spectroscopy using NO as a probe molecule. Prepared samples have been studied, as well as samples pretreated in different ways, since the activation influences both the structure and the catalytic properties of the materials. Because of their interesting structural features and because they show the highest activity in the selective catalytic reduction of NO_x, most attention has been paid to the samples prepared by aqueous exchange.

2. Experimental Section

2.1. Preparation Procedures. Catalysts were made from the ammonium or sodium forms of the parent zeolite with a nominal framework Si/Al ratio of 33, supplied by Catal Ltd, (Sheffield, England). The framework Si/Al ratio was determined by ^{29}Si MAS NMR to be 34 ± 2, using a Bruker spectrometer operating at 500 MHz and a spinning speed of 25 kHz.

Fe−ZSM-5 catalysts have been prepared by four different methods: exchange from aqueous solution, exchange from methanolic solution, exchange by the special technique reported by FH, and exchange in the solid state. Aqueous ion exchange was carried out in a single exchange step at pH 5−6, with solutions of various concentrations (10^{-2}, 10^{-3} mol L^{-1}) of iron(III) nitrate nonahydrate (Aldrich Chemical, >99.99% pure). The sample (2 g) was stirred at room temperature, and argon was bubbled through approximately 150 mL of the solution at a flow rate of 5 L/h. Because iron oxy−hydroxide species present in aqueous solution are thought to be inimical to exchange (see below), samples were also prepared by ion exchange in methanol solution. Iron(III) nitrate was dissolved in absolute methanol and then dried with water-free calcium sulfate to remove the water of crystallization. The solution was filtered and mixed with the dried zeolite (20 g L^{-1}). To exclude water vapor from the exchange vessel, dry nitrogen was bubbled through the slurry, which was also irradiated in a 360 W ultrasonic bath. The FH approach is to carry out exchange from Fe(II) rather than Fe(III), using a glass sinter to prevent the access of oxy−hydroxide species to the zeolite. Fe(II) oxalate is used, since the oxalate ion is more easily oxidized by molecular oxygen to CO_2 than is aqueous Fe(II) to Fe(III). Again, argon has been bubbled through the solutions at a rate of 5 L/h and the solution was stirred over a peroid of 24 h. Iron(II) oxalate (1 g) was slurried in water with 2 g of the zeolite. Samples have been prepared from both sodium and proton forms of the zeolite to test for any influence of the cations present on the stability of the exchanged catalysts. Attempts to prepare solid-state-exchanged samples involved grinding the zeolite with the iron salt under nitrogen in a glovebox (see Table 1) followed by heat treatment before use, as described below. Iron(II) chloride, 0.126 g (Avocado, 99% purity), or iron(II) carbonate, 0.073 g (ABCR), and 2 g of ZSM-5 were ground together in an agate mortar for about an hour.

2.2. Characterization. The iron content of the materials has been determined by atomic absorption spectroscopy, and they were subsequently characterized by temperature-programmed reduction, in situ X-ray absorption spectroscopy (EXAFS and XANES), infrared spectroscopy, and electron microscopy. For TPR, approximately 50 mg of catalyst was preheated to 820 K in flowing dry air or nitrogen for 1 h, cooled to room temperature, and then heated in a 40 mL min^{-1} flow of 5% hydrogen in argon at 5 K min^{-1}. Hydrogen uptake was measured by a thermal conductivity detector. X-ray absorption spectroscopy was carried out using wiggler radiation on beamline 9.3 at the CCRL Daresbury Laboratory, in an in situ cell to be described in detail elsewhere,[16] and the EXAFS results were analyzed using standard procedures.[17] The statistical significance of each shell of neighbors reported has been confirmed by the standard test.[18] All X-ray absorption spectra were measured in fluorescence mode by a multielement, energy-sensitive Canberra solid-state detector. For infrared spectroscopy, samples were pressed into thin self-supporting wafers weighing ca. 20 mg, and measurements were performed using an ATI RS1 Fourier transform spectrometer equipped with an in situ stainless steel cell with calcium fluoride windows, capable of a base pressure $<10^{-7}$ mbar. Where necessary, the intensity of spectral features was fitted using the GRAMS 386 peak fitting routine. Peak fitting used a mixed Gaussian/Lorentzian line shape with a Gaussian/Lorentzian ratio of 0.3, and height, position, and width were unconstrained. X-ray photoelectron spectroscopy was carried out with a VG ESCA 3 spectrometer, which has been described previously,[8] using Mg Kα radiation. Binding energies were determined relative to the adventitious carbon impurity, with the carbon 1s binding energy taken to be 285.0 eV, and no evidence of reduction in the X-ray beam was noted. The energy dependence of the spectrometer transmission function was determined by measuring the photoelectron peaks from a cleaned silver foil and using excitation cross sections due to Schofield.[19] High-resolution electron microscopy was performed in an JEOL 200EX microscope operating at 200 keV, with the samples supported on holey carbon grids. Catalytic measurements were carried out in a flow apparatus with chemiluminescent NO_x detection and gas chromatography, and that has

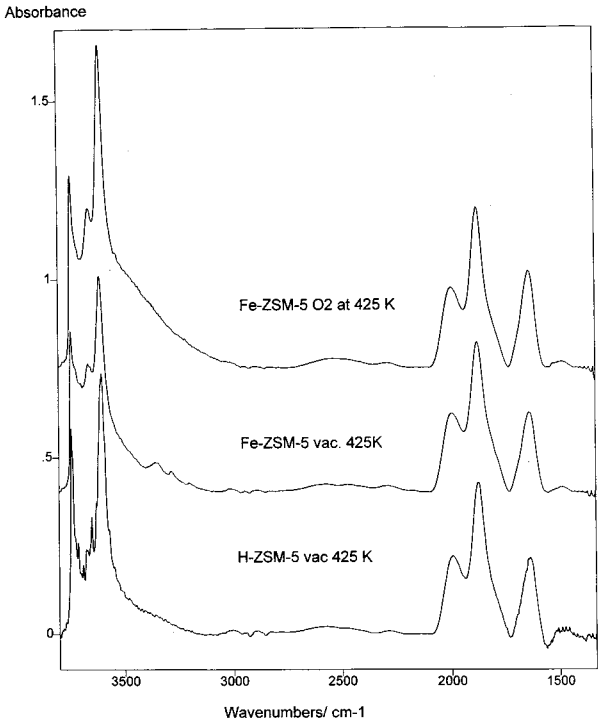

Figure 1. Infrared spectra measured at 425 K after pretreatment at 773 K: (lowest curve) the parent ZSM-5 after treatment in vacuo; (middle curve) Fe−ZSM-5 prepared by aqueous exchange, after treatment in vacuo; (upper curve) the same material after treatment in 10 mbar oxygen.

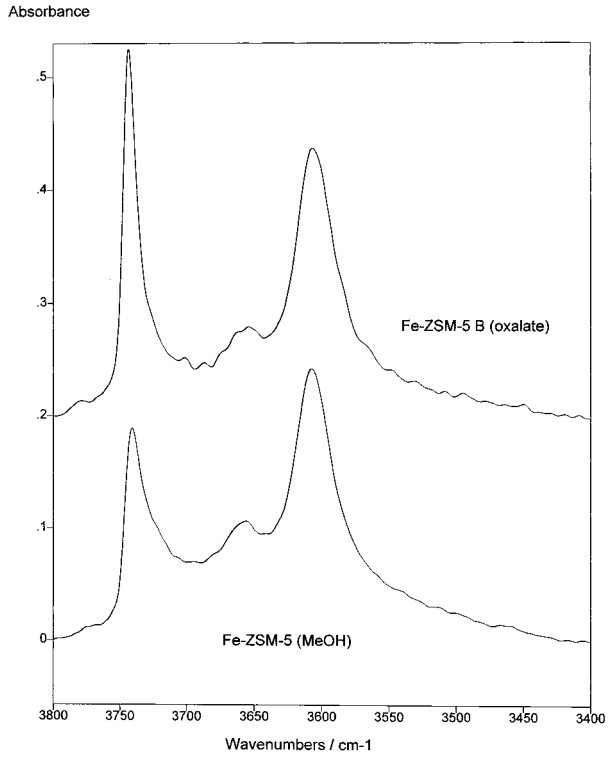

Figure 2. Infrared spectra measured at 425 K after pretreatment in vacuo at 773 K: (lower curve) Fe−ZSM-5 prepared by exchange in methanol; (upper curve) Fe−ZSM-5 prepared by the method of Feng and Hall (see text).

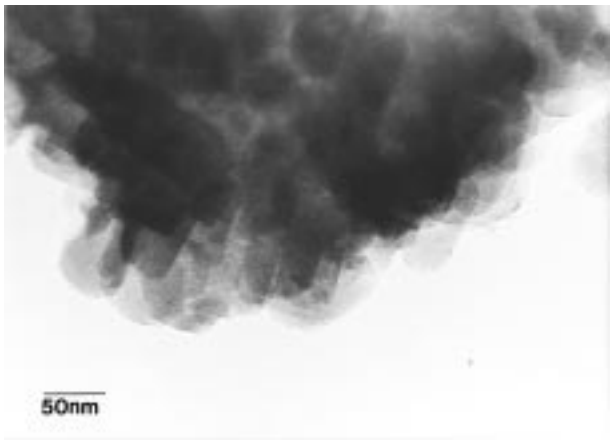

Figure 3. Electron micrograph of Fe−ZSM-5 prepared by aqueous exchange and calcination in air at 773 K.

also been described previously.[20] The NO concentration was 2000 ppm; propene was used as the model hydrocarbon at a concentration of 1000 ppm, with 2% oxygen and helium as an inert diluent. The catalyst mass was typically 0.25 g, and the gas hourly space velocity was 30 000 h^{-1}.

3. Results

Table 1 indicates the samples that have been studied, together with their concentrations of iron, tetrahedral aluminum, and protons. The concentration of protons was determined by quantitative infrared spectroscopy of the −OH band at ca. 3610 cm^{-1}. To achieve quantification, the intensity of this band was normalized for varying wafer thickness using the intensity of the zeolite overtone bands at 1878 and 1933 cm^{-1} [21] and was standardized using a sample from which the concentration of tetrahedral aluminum, and therefore of protonic OH groups, was known from MAS NMR measurements.

3.1. Infrared Spectroscopy of the OH Stretching Vibration Region. The infrared spectrum of the zeolite provides a quantitative indication of the extent to which introduction of iron affects the presence of Brønsted acidity. Figure 1 shows infrared spectra, measured at 425 K, of the parent H−ZSM-5 and of samples of Fe−ZSM-5 prepared by aqueous exchange after activation at 773 K either in a vacuum or in oxygen. Comparisons are made at this temperature to avoid adsorption of water traces. Figure 2 shows IR spectra of samples prepared by exchange from methanol and by the FH procedure. Samples exhibit the expected bands in the OH stretching vibration region; that at 3670 cm^{-1} is assigned to extraframework species,[22] those at 3600−3610 cm^{-1} to bridging, acidic hydroxyl stretching vibrations, and that at 3740 cm^{-1} is attributed to stretching vibrations of terminal Si−OH groups.[23]

3.2. Characterization of the Zeolite Surface and of the Iron Spatial Distribution. For metal-exchanged zeolites it is always important to have information on the extent to which the metal may be concentrated at or near the external surface. This is particularly important for iron-containing materials because of the complexity of that metal's aqueous chemistry, as emphasized by FH.[14] We have used both transmission electron microscopy combined with elemental analysis and XPS to study the distribution of iron-containing species through our samples. Figure 3 shows a typical electron micrograph of an aqueous-exchanged sample calcined in the absence of oxygen. The appearance of particles of approximate dimension of 2 nm at the external surface of the zeolite should be noted. EDAX analysis, which in the instrument used does not detect oxygen, showed that these particles contain both iron and silicon, with an Fe/Si ratio of approximately 5.7:1. This ratio implies that these particles are a mixture of iron oxides and silicates. Importantly, EDAX analysis also confirms the presence of iron

TABLE 2: X-ray Photoelectron Spectroscopy Results for Fe−ZSM-5

sample	Fe/Si bulk ratio[a]	Fe/Si ratio based on Fe $2p_{3/2}$ peak	Fe/Si ratio based on Fe 3p peak	Fe $2p_{3/2}$ binding energy (eV)
Fe−ZSM-5 (air)	7.9×10^{-3}	3.6×10^{-2}	1.5×10^{-2}	711.7
Fe−ZSM-5 (Ar)	7.9×10^{-3}	1.6×10^{-2}	7.3×10^{-3}	712.0

[a] From atomic absorption spectroscopy.

within the main body of the zeolite crystals, with an Fe/Al molar ratio of approximately 0.5.

The depth distribution of iron has also been probed by XPS, which has been shown to be a good method of establishing whether transition metals are preferentially located at the zeolite external surface. For low-density materials such as zeolites, XPS probes at least 30 Å into the bulk of the material. When surface segregation occurs, as for example in the case of a Cu−ZSM-5 catalyst prepared by impregnation, the metal/silicon ratio observed by XPS exceeds the bulk value significantly, in the example cited by a factor of about 30.[24] Table 2 gives the Fe/Si XPS ratios measured for aqueous-exchanged samples pre-

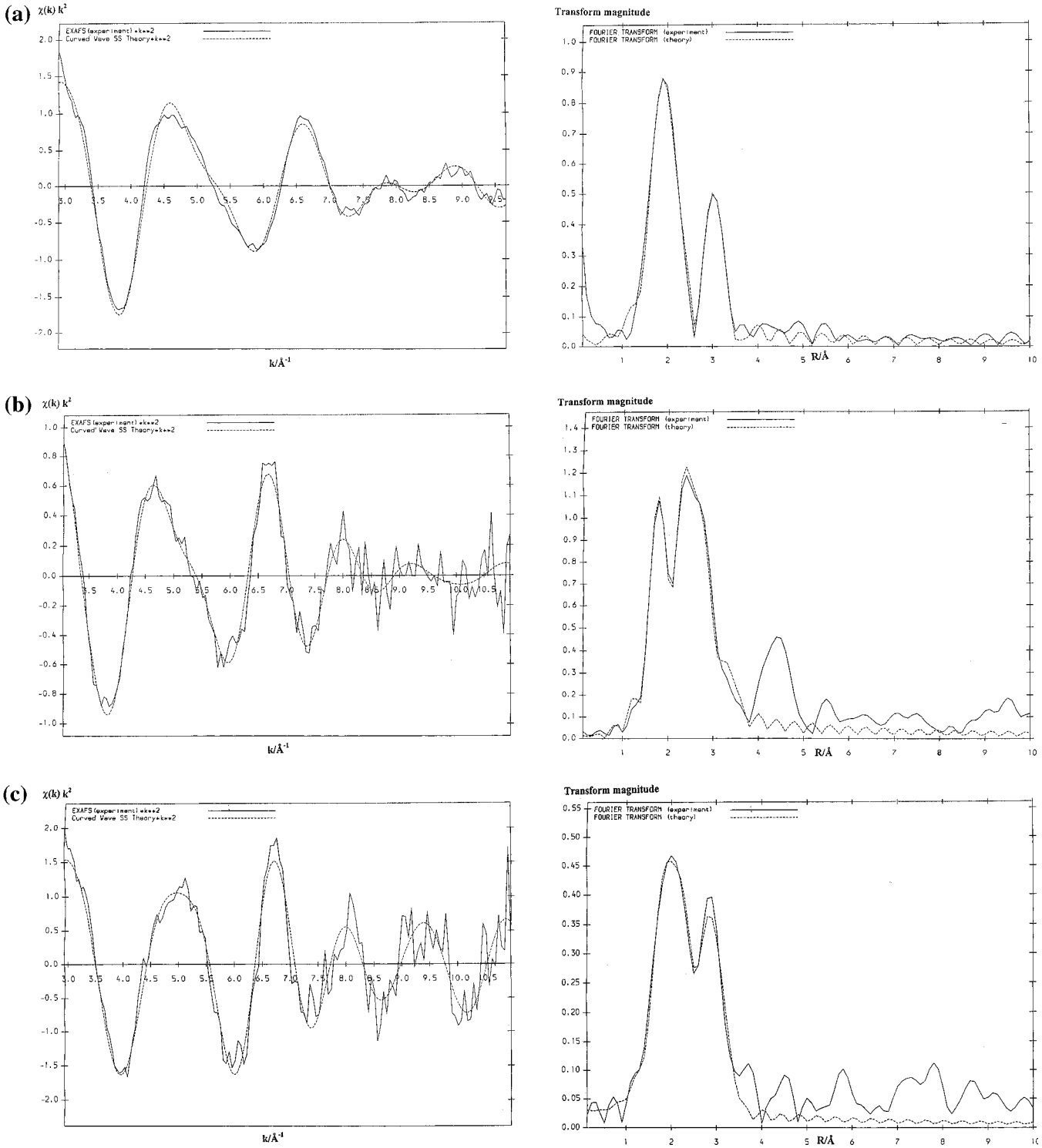

Figure 4. Reciprocal space and real space (Fourier transform) EXAFS spectra: (a) experimental (solid line) and calculated EXAFS spectra (dashed line) of prepared Fe−ZSM-5; (b) EXAFS spectra of Fe−ZSM-5 prepared by aqueous exchange followed by in situ calcination He/O_2 at 655 K; (c) as in (b) but calcined in nitrogen.

TABLE 3: Results of in Situ EXAFS Studies of Fe−ZSM-5[a]

	Fe−O		Fe−O		Fe−Fe		Fe−Si	
sample & pretreatment	*N*	*R*/Å	*N*	*R*/Å	*N*	*R*/Å	*N*	*R*/Å
Fe−ZSM-5-50%, as prepared	0.9	1.93	5.3	2.03	1.4	3.00	1.3	3.37
Fe−ZSM-5, heated in N_2 at 655 K	2.1	1.95	2.2	2.13	2.9	2.53	1.9	3.18
Fe−ZSM-5, as above followed by heating in H_2 at 655 K	1.2	1.94	3.6	2.11	1.4	2.51	1.0	3.24
Fe−ZSM-5, after heating in O_2 at 655 K	1.8	1.87	3.9	2.02	1.9	2.53	2.2	3.23
Fe−ZSM-5, as above followed by heating in H_2 at 655 K			3.1	2.04	2.0	2.53	1.0	3.26
Fe−ZSM-5, (FH) as prepared			6.1	2.13	1.0	2.47		
Fe−ZSM-5, prepared by exchange in MeOH followed by N_2 at 655 K			5.1	2.10	1.4	2.49		

[a] For details see text. Coordination numbers (*N*) are accurate to ±10% and interatomic distances (*R*) to ±0.02 Å. Debye−Waller factors are typically in the range 0.005−0.025 Å^2.

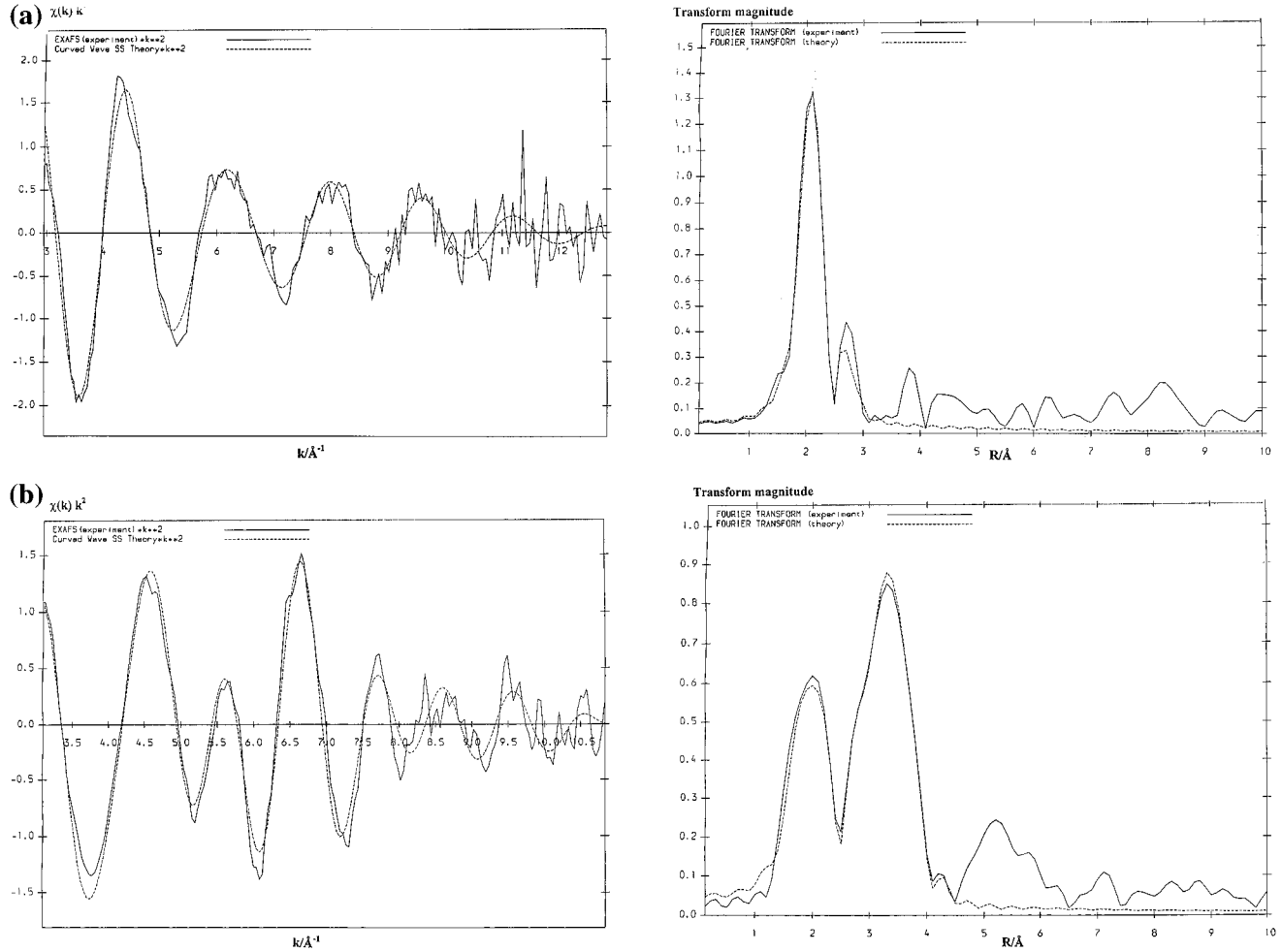

Figure 5. Reciprocal space and real space (Fourier transform) EXAFS spectra: (a) experimental (solid line) and calculated EXAFS spectra (dashed line) of Fe−ZSM-5 prepared by the method of Feng and Hall; (b) as in (a) but after in situ calcination at 655 K.

treated in argon and in air and determined by taking the Fe 3p and Fe $2p_{1/2}$ peaks and the Si 2p peak and applying standard quantification equations and cross sections.[19] The iron-to-silicon surface ratios obtained from considering the two different iron peaks differ by about a factor of 2. We do not understand this, although the same discrepancy can be found by comparing photoelectron spectra of identical Fe−ZSM-5 materials reported by Kaliaguine et al. in refs 25 and 26. In the first of these references the authors report a value of Fe/Si = 0.046, calculated using the Fe 3p peaks, while in ref 26 *for the same sample* they quote an Fe/Si ratio of 0.118, this time on the basis of Fe $2p_{3/2}$ peak areas. However, despite this problem of quantification, the results in Table 3 show that there is little surface segregation. For the sample calcined in argon, which is of the greatest structural and catalytic interest, the surface iron/silicon ratio determined by XPS either equals the bulk value or only exceeds it by a factor of 2, depending on which iron peak is chosen.

3.3. EXAFS Spectroscopy. The samples prepared by aqueous exchange have been thoroughly examined by in situ X-ray absorption spectroscopy, both EXAFS and XANES. The Fe K edge EXAFS results, which provide information on the structural environment of the iron in the sample, are considered first. Figure 4a shows both the experimental and calculated reciprocal space and real space (Fourier transform) spectra for a *prepared sample*. The parameters used in this and subsequent calculations are listed in Table 3. Figure 4b shows the experimental and calculated EXAFS of the same material, measured at room temperature after treatment in He/O_2 at ca. 655 K. Experimental and calculated iron K edge EXAFS for a sample pretreated in

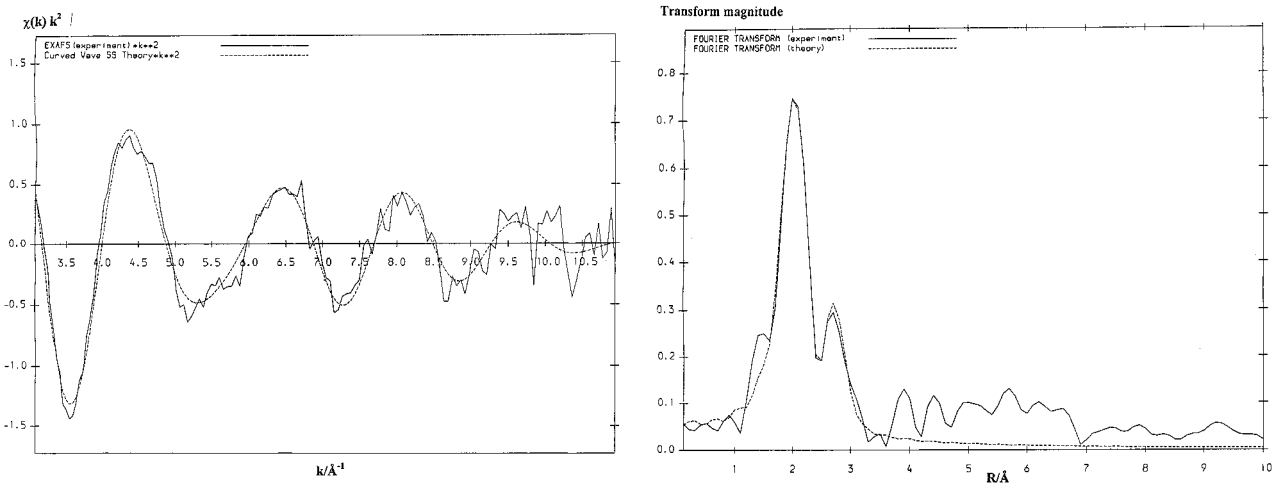

Figure 6. Reciprocal space and real space (Fourier transform) EXAFS spectra: experimental (solid line) and calculated EXAFS spectra (dashed line) of Fe−ZSM-5 prepared by exchange in methanol followed by in situ calcination in nitrogen at 655 K.

nitrogen to the same temperature are shown in Figure 4c. Parts a and b of Figure 5 show results for a prepared sample exchanged by the FH method and the same sample treated in nitrogen at 773 K, respectively. It is interesting to note that although the spectrum of the prepared sample largely indicates isolated iron atoms, calcination leads to the extensive formation of Fe_3O_4 aggregates, which are likely to be at the external surface. Results for a sample exchanged from methanol solution and after pretreatment in nitrogen are plotted in Figure 6. Some EXAFS results obtained after heating the catalysts in hydrogen are also summarized in Table 3.

3.4. Stability and Redox Behavior. The stability of the different oxidation states of iron in these materials is of considerable interest in view of their possible catalytic applications, so we have probed their redox behavior using XANES, TPR, and XPS and by employing NO as a probe molecule followed by IR spectroscopy. Figure 7 shows X-ray absorption near-edge spectra for samples prepared by aqueous exchange and subjected to a variety of treatments, as well as XANES of a number of iron reference compounds. XANES is essentially a fingerprint technique, allowing the oxidation state and coordination environment to be identified if a suitable model compound is available. Figure 8a shows the first derivative of the XANES spectra with iron in oxidation state +3, while Figure 8b shows some derivative spectra of samples with iron in oxidation state +2. Both plots include FeO and Fe_2O_3 to aid comparison.

Temperature-programmed reduction was performed on a number of samples, with copper(II) oxide used as a calibrant, and the results are shown in Figure 9. Fe−ZSM-5 pretreated in the presence of oxygen exhibited only a small reduction feature at approximately 750 K. Samples prepared by anaerobic exchange in the FH procedure and by solid-state iron exchange, however, exhibit significant reduction features at ca. 640−850 K.

Nitric oxide was adsorbed on materials prepared by aqueous exchange but with different pretreatment histories, and FTIR results are presented as normalized difference spectra. Figure 10a gives spectra obtained at 303 K and 1×10^{-3} mbar NO pressure for a range of samples, and Figure 10b shows the result of increasing the NO pressure to 10 mbar over Fe−ZSM-5 pretreated in a vacuum. At 10^{-3} mbar, the main features are a major band at 1880 cm^{-1}, shoulders at 1860 and 1841 cm^{-1}, and a weak band at 1771 cm^{-1}. At 10^{-2} mbar, discrete new bands appear at 1815 and 2250 cm^{-1}, the band at 1815 cm^{-1}

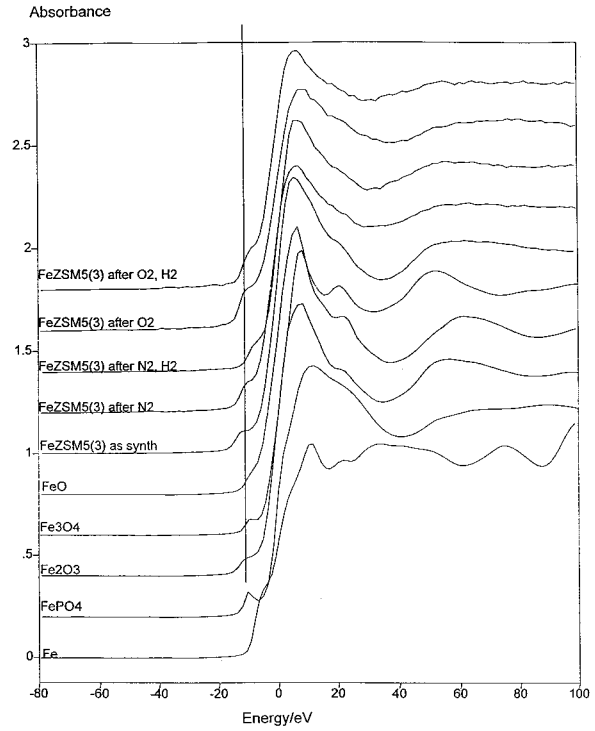

Figure 7. X-ray absorption near-edge spectra (XANES) of Fe−ZSM-5 samples prepared by aqueous exchange and subject to the indicated pretreatments. Spectra of a number of iron compounds are also shown for comparison purposes. The energy zero chosen is that of the first preedge inflection point of metallic iron at 7112 eV.[55]

gains intensity, and the shoulder at 1860 cm^{-1} is slightly increasing in intensity. Raising the pressure to 1 mbar causes an increase of the intensity of the bands at 1815, 2135, and 2250 cm^{-1}. Significant changes to the spectrum occur when the NO pressure is increased from 1 to 10 mbar. The bands at 1815, 2250 cm^{-1} and the shoulder at 1860 cm^{-1} *decrease* in intensity, but the feature at 2135 cm^{-1} increases dramatically, as do the bands in the region 1500−1680 cm^{-1}. It is important to note that the band at 1880 cm^{-1} stays constant in intensity during a pressure increase from 10^{-3} to 10 mbar for all samples studied. Subsequent removal of gas-phase NO results in decreasing intensity at 1815, 1860, and 2135 cm^{-1}.

To aid the assignment of the IR spectra, a sample has been prepared by aqueous exchange but containing about half the iron concentration of the samples studied to date, designated

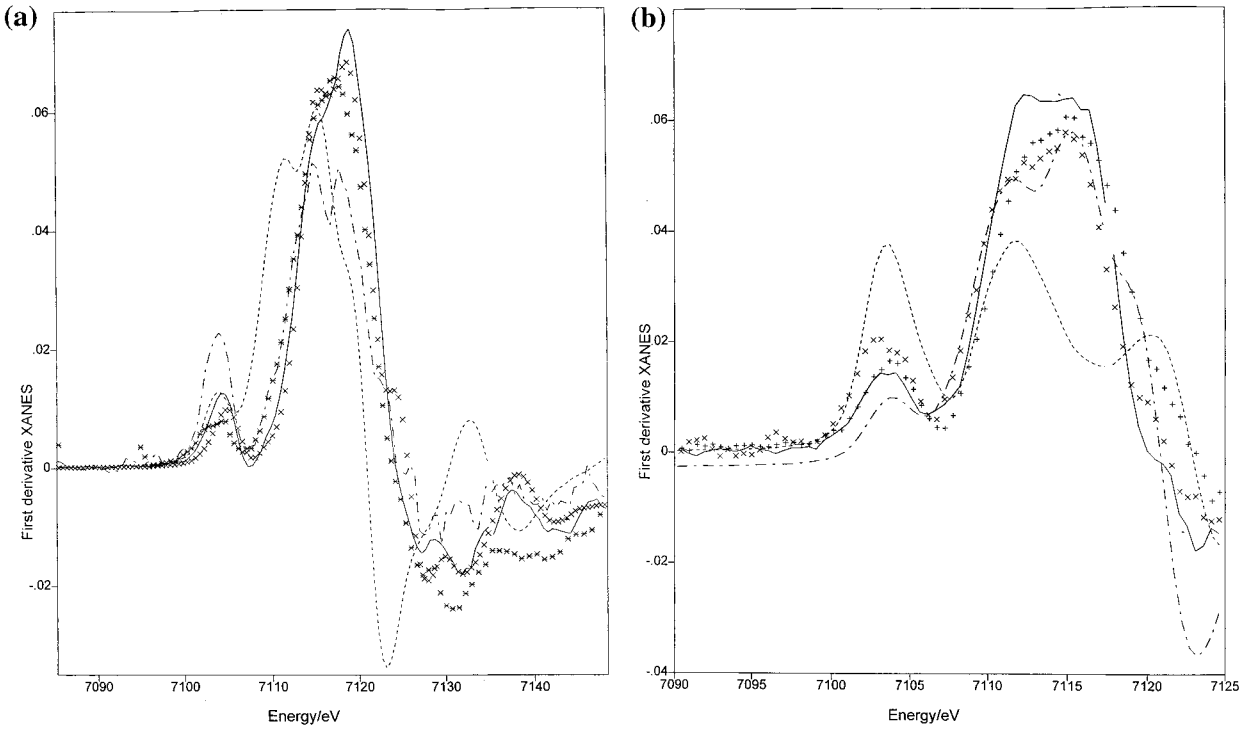

Figure 8. First-derivative XANES. (a) Samples believed to be in the +3 oxidation state: prepared by aqueous exchange (solid line); as previous, after activation in oxygen at 655 K (dash/dotted line); prepared by exchange in methanol (asterisk); iron(III) oxide (cross); iron(II) oxide for comparison (dashed line). (b) Samples in the +2 oxidation state: iron(II) oxide (dashed/dotted line); prepared by aqueous exchange followed by heating in nitrogen at 655 K (cross); as previous, followed by heating in hydrogen at 655 K (solid line); prepared by aqueous exchange followed by heating in oxygen at 655 K and then in hydrogen at the same temperature (×); metallic iron (for comparison) (dashed line).

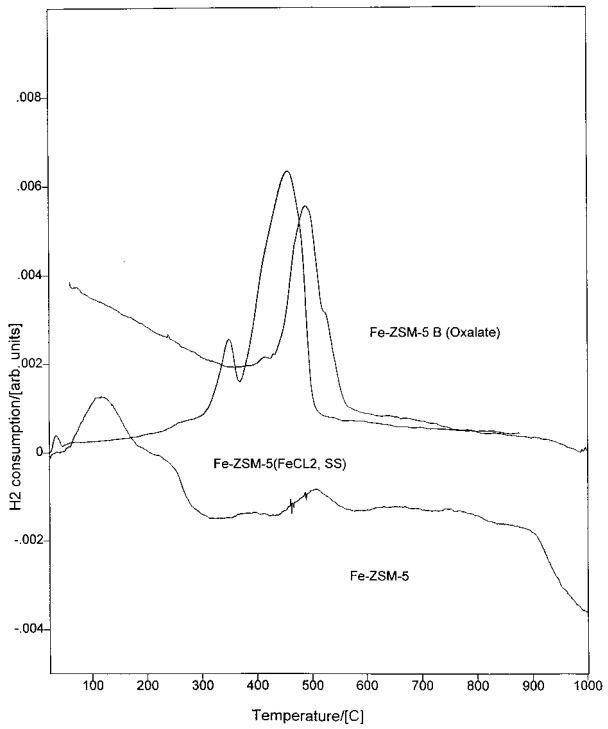

Figure 9. Temperature-programmed reduction results for Fe−ZSM-5 materials prepared in different ways, obtained after pretreatment in air at 775 K for 1 h.

Fe−ZSM-5-50%. The main spectral feature of NO adsorbed at 10^{-3} mbar on this sample is again a band centered at 1880 cm^{-1} but with shoulders at 1841 and 1860 cm^{-1}. For direct comparison, Figure 11a shows spectra of two samples with the different iron content, measured at 10^{-2} mbar pressure. Figure 11b shows the influence of pretreament conditions on Fe−ZSM-5-50%. The intensity of the bands at 2135 and 1627 cm^{-1} is higher after calcination in oxygen. NO adsorption at 10 mbar results in a behavior similar to that found at higher iron loadings, but the intensities of the bands at 2133 and 1880 cm^{-1} are lower. Of the other samples studied, the spectra resulting from NO adsorption were similar to those already described, but the intensities of bands varied between samples, as indicated in Tables 4 and 5.

3.5. Catalytic Activity. Figure 12a shows the performance in the selective catalytic reduction reaction for Fe−ZSM-5 samples pretreated in the presence and in the absence of oxygen. In both cases selectivity is exclusively to nitrogen, but it is important to note that the sample pretreated in the *absence* of oxygen shows significantly larger conversion of NO_x than that pretreated in He/O_2. Materials prepared by methanolic exchange exhibit conversions similar to those activated anaerobically, as shown in Figure 12b. Samples prepared by the FH methods show catalytic behavior similar to that of aqueous-exchanged Fe−ZSM-5-activated in the *presence* of oxygen, as shown in Figure 12c.

The temperature for maximum NO_x conversion for the best iron-containing materials is similar to that observed for the more extensively studied Cu−ZSM-5 system; however, the absolute rates are significantly lower for Fe−ZSM-5.[20] This is not surprising, taking into account the low iron content compared to Cu, where loadings of >3% weight are readily achievable. The turnover frequencies for the best iron catalysts typically exceed those noted for copper[27] by about a factor of 2.

4. Discussion

We first discuss the extent to which iron is exchanged into ZSM-5 by the various methods used and the oxidation states that are observed. The consequences of different activation procedures and the iron-containing structures that are formed are then considered followed by a discussion of the results of

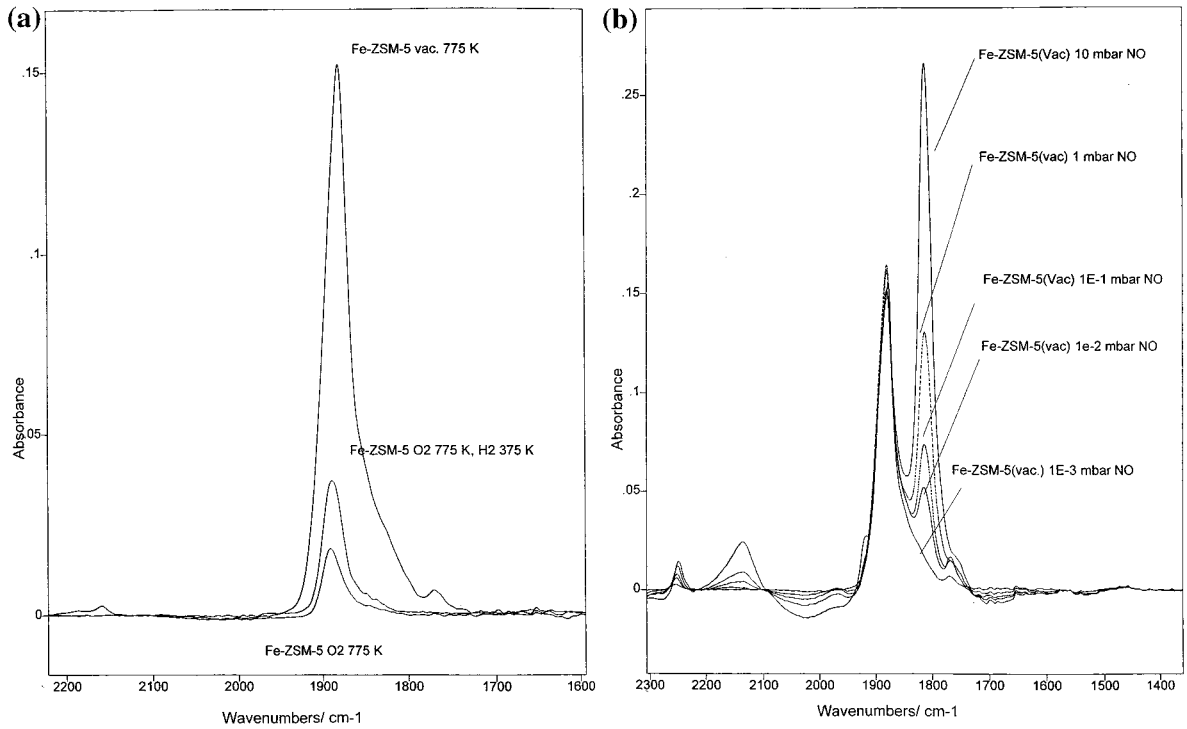

Figure 10. FTIR spectra measured at 303 K: (a) at 1×10^{-3} mbar of nitric oxide; (b) showing the result of increasing the NO pressure to 10 mbar over Fe−ZSM-5.

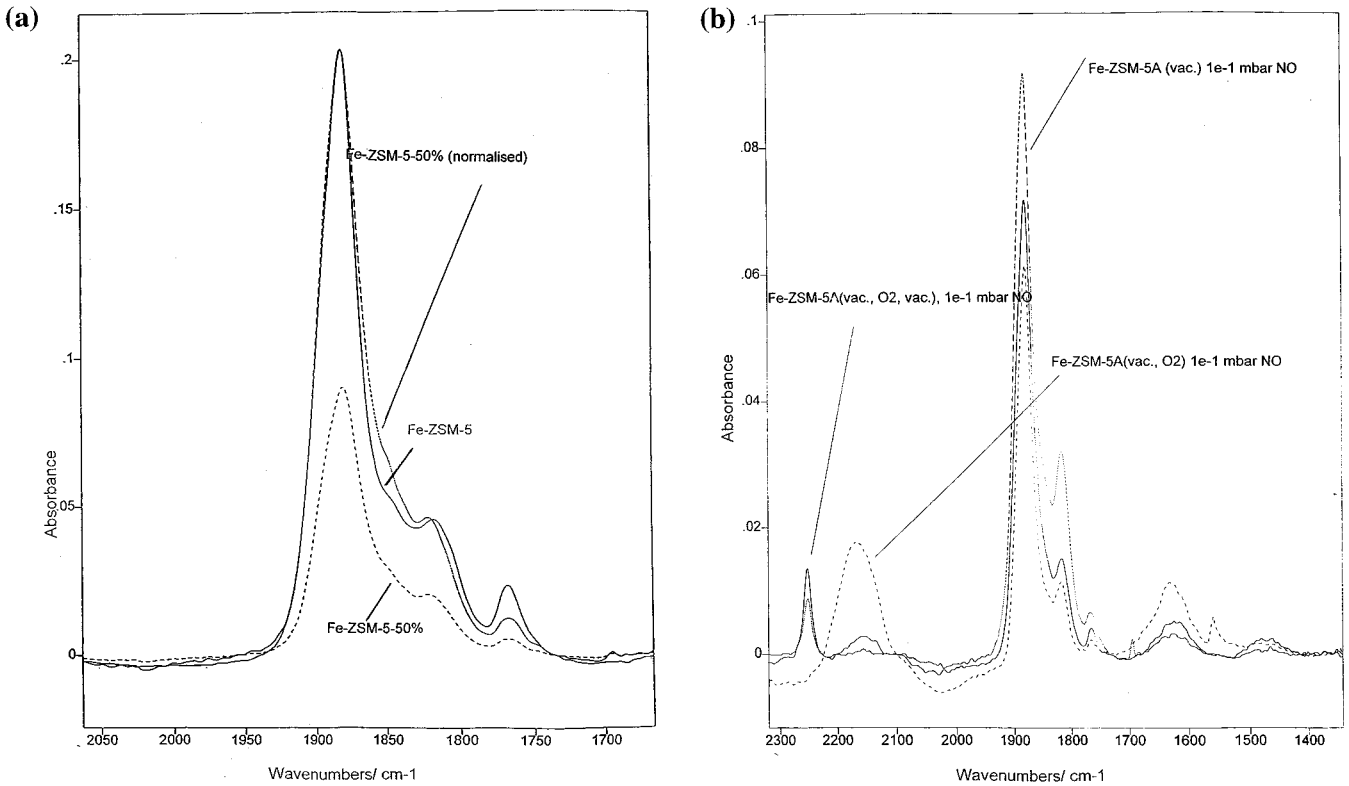

Figure 11. (a) FTIR spectra of samples containing different amounts of iron (see text) prepared by aqueous exchange. Samples were pretreated in vacuo and exposed to 1×10^{-2} mbar NO. The upper dashed curve is for Fe−ZSM-5-50% normalized in intensity to that of the most intense band in Fe−ZSM-5 to aid visual comparison. (b) Spectra showing the influence of pretreatment conditions on Fe−ZSM-5-50%.

nitric oxide adsorption. Last, we examine the behavior of these materials in the selective catalytic reduction of NO_x and speculate on ways in which the *iron−oxo nanoclusters* interact with the ZSM-5 zeolite.

4.1. Prepared Samples: Extent of Exchange and Oxidation State. Table 1 shows that the maximum amount of iron introduced into ZSM-5 by the various preparation methods used does not exceed the theoretical value for 100% exchange, calculated using an Fe/Al ratio of 0.33, except where solid-state exchange was attempted. This is in agreement with previous reports for ZSM-5,[28] and also with findings on mordenite[29] and faujasite,[30,31] but is significantly different from copper- and cobalt-exchanged materials,[32] where overexchange is readily achievable. Furthermore, studies of the changes in

TABLE 4: Relative Amounts of NO Adsorption on Fe−ZSM-5 Samples Pretreated in Different Ways, Measured at 303 K and $P_{NO} = 10^{-3}$ mbar[a]

sample & pretreatment	absorbance
Fe−ZSM-5: vacuum, 775 K	1
Fe−ZSM-5: O_2, 775 K	0.10
Fe−ZSM-5: O_2, then vacuum, 775 K	0.15
Fe−ZSM-5: O_2, 775 K; H_2, 375 K	0.19
Fe−ZSM-5-50%: vacuum, 775 K	0.48
Fe−ZSM-5-50%: vacuum, 775 K; O_2, 775 K	0.11
Fe−ZSM-5-50%: vacuum, 775 K; O_2, 775 K; vacuum, 775 K	0.35
Fe−ZSM-5 (oxalate): vacuum, 775 K	0.48
Fe−ZSM -5, (MeOH): vacuum, 775 K	0.79

[a] The absorbances of the main infrared bands due to NO, at 1880 and 1841 cm^{-1}, have been integrated together and normalized.

TABLE 5: Relative Amounts of NO Adsorption on Fe−ZSM-5 Samples Pretreated in Different Ways, Measured at 303 K and $P_{NO} = 10^{-2}$ mbar

sample and pretreatment	absorbance at 1814 cm^{-1}	absorbance at 1860 cm^{-1}
Fe−ZSM-5: vacuum, 775 K	1	0.41
Fe−ZSM-5: O_2, vacuum, 773 K	0.06	0.03
Fe−ZSM-5-50%: vacuum, 775 K	0.4	0.35
Fe−ZSM-5 (MeOH): vacuum, 775 K	0.9	1.78

intensity of the protonic OH infrared band, which are also summarized in Table 1, show that in all cases the number of protons displaced by iron introduction is much lower than would be expected from a simple exchange process, again indicating significant differences between iron and other first-row transition metals. These well-recognized difficulties in achieving straightforward exchange of iron into zeolites are assigned to the more complex aqueous chemistry of this metal[33] and specifically the formation of hydrous iron oxides in the pH ranges necessary; here, pH = 6. The $Fe(III)(H_2O)_6$ complex is stable only at pH $\approx$ 0,[34] where severe leaching of the aluminum of the zeolite would occur.

In an attempt to prevent formation of aggregated oxy−hydroxide species, and therefore to maximize the degree of ion exchange, we have performed preparations using carefully dried iron(III) nitrate dissolved in methanol. Even after refluxing of the ZSM-5/methanol slurry, only approximately 10% exchange was achieved. However, in combination with ultrasonic irradiation, we were able to exchange 80% of the bridging −OH groups of the zeolite in a single step. A control experiment confirmed that ultrasound does not degrade the proton content of the zeolite; when a slurry of H−ZSM-5 in methanol was treated with ultrasonic radiation, no decrease of the concentration of bridging OH groups in the zeolite occurred.

The approach to exchange developed by FH is also designed to avoid problems due to formation of iron oxy−hydroxides,[14] and in our hands we achieve a high iron content (Table 1). Infrared and EXAFS results taken together suggest that the prepared FH material contains isolated oxalate species that are probably well dispersed within the pore structure. However, after heat treatment at 773 K the infrared bands associated with oxalate species disappear, and the EXAFS and XANES results indicate the presence of relatively large clusters of Fe_3O_4, which must be at the external surface of the zeolite.

In a further attempt to increase the iron content of these materials, a number of preparations aimed at achieving solid-state ion exchange have been carried out, as indicated in Table 1. Despite using both Fe(II) and Fe(III) salts and a range of anions, as well as aerobic and anaerobic conditions, the extent of proton exchange did not exceed that achieved by aqueous

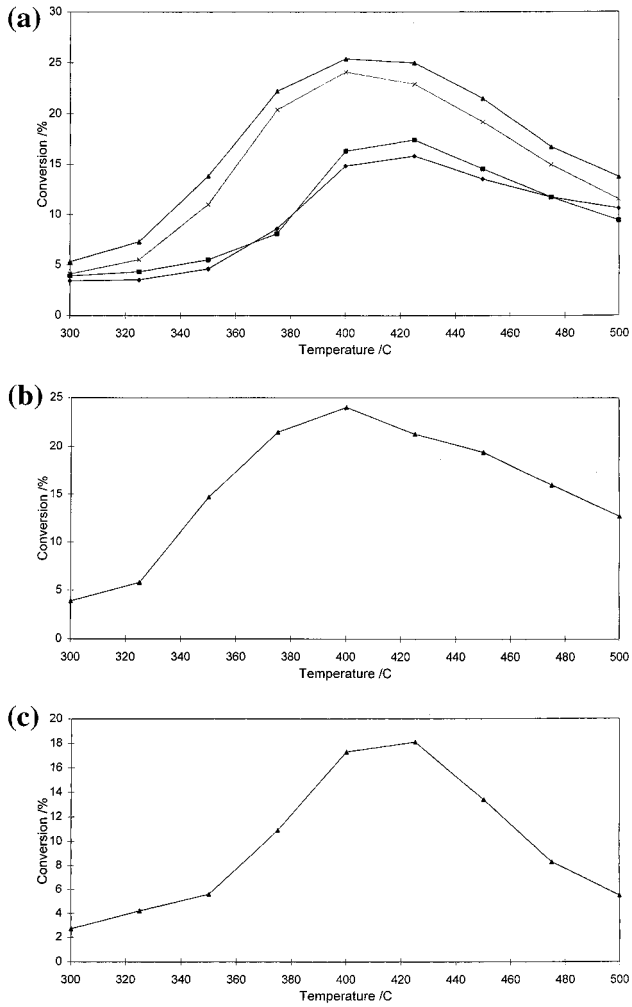

Figure 12. Nitric oxide conversion as a function of temperature over Fe−ZSM-5 under conditions indicated in the text. (a) Catalysts prepared by aqueous exchange: (triangle) activated in helium at 775 K; (cross) activated in helium followed by oxygen at 775 K; (diamond) activated in oxygen at 775 K; (square) activiated in oxygen followed by helium at 775 K. (b) Catalyst prepared by exchange in methanol, pretreated in an inert atmosphere. (c) Catalyst prepared by the FH method, pretreated in the absence of oxygen.

methods. Since these materials have high iron loadings, it is clear that this approach is predominantly effecting impregnation rather than exchange, and so these materials are not considered further.

XANES measurements indicate that, as expected, iron is present in the +3 oxidation state in the prepared materials. Figures 7 and 8 show that there is a shift of ca. 3 eV in the position of the iron K edge between FeO and Fe_2O_3 and that the zeolite XANES is very similar to that of iron(III) oxide. The preedge peak at 7104 eV is assigned to a 1s-to-3d-like transition, which is forbidden in pure octahedral symmetry but becomes allowed under distortions from octahedral symmetry or in tetrahedral symmetry.

EXAFS results for the prepared samples are summarized in Table 3, and by comparison with known Fe−O and Fe−Fe distances,[35] the results suggest the presence of small FeOOH or possibly Fe_2O_3 clusters. The Fe−Fe coordination number is small (1.5), indicating that the average cluster contains between two and three iron atoms.

4.2. Fe−ZSM-5 Activated in the Absence of Oxygen. Catalysts activated in an oxygen-free atmosphere (vacuum, nitrogen, or helium) show some of the most interesting structural

and catalytic properties and so are considered first. Both XANES (Figure 8) and TPR measurements suggest that autoreduction of the iron occurs during this treatment so that the iron is converted to the +2 oxidation state. The position and shape of the edge structure are similar to that of FeO, and the TPR does not show the feature attributed to the reduction of Fe(III) to Fe(II) in the oxygen-treated catalyst (see below).

An important feature of the samples prepared by aqueous and methanolic exchange is their stability against reduction below the +2 oxidation state. For samples pretreated in nitrogen, TPR shows that no significant reduction occurs up to 1250 K (Figure 9), and the stability against reduction is supported by XANES measurements in hydrogen, which could only be carried out to 655 K. Difficulty in reducing all of the iron in conventional supported catalysts is well-known, suggesting that very small metal−oxo clusters of the type present here (see below for discussion of the EXAFS results) are very stable.[36] Support for this conclusion is provided by TPR results of iron-exchanged faujasites, where reduction to metallic iron occurs only at 1300 K, after breakdown of the zeolite lattice.[30]

Catalysts prepared by procedures intended to induce solid-state exchange undergo reduction to metallic iron at 790 K, suggesting the presence of much larger clusters and again indicating that this approach has in our hands produced results much closer to impregnation. The FH materials also undergo reduction to Fe(0) at 695 K; this is the behavior expected of the large iron oxide clusters known from EXAFS to be present in this material after heating to 775 K.

As already discussed and as emphasized by FH, for iron−ZSM-5 materials it is important to establish that the iron species exist predominantly within the pore structure of the zeolite and not at the external surface. Both the surface region Fe/Si ratios determined by XPS and the EDAX mapping of the catalysts treated in an inert atmosphere show that this is the case, although TEM does detect some discrete particles at the external surface.

EXAFS reveals an intriguing structural picture about the small clusters. Calcination of the prepared materials in nitrogen (Figure 4c) causes an increase in the iron−oxygen interatomic distance, as shown in Table 3, while the coordination number decreases from ca. 6 to 4. The increase in the Fe−O distance, compared to both the parent sample and that pretreated in oxygen, is an indication of reduction to Fe^{2+}, since the Fe^{2+} ion is larger than the Fe^{3+} ion. A more important difference compared to the prepared materials is the observation of the nearest-neighbor iron−iron distance of 2.53 ± 0.02 Å. This is a very unusual distance for an iron oxide system, since in bulk oxides the smallest Fe−Fe distance reported is 2.89 Å for α-Fe_2O_3,[37] and values of ca. 3 Å are the norm. Very short iron−iron distances have been found after pretreatment in all of the samples studied by EXAFS (Table 3), so the origin of this structural feature must be considered in some detail.

The nearest-neighbor distance in body-centered cubic metallic iron is 2.48 Å, and similar Fe−Fe distances have been reported in EXAFS studies of iron carbonyl derived, alumina-supported materials after reduction.[38] It is important to note that these disappeared on oxidation of the catalysts. In the present materials, however, we have already cited good evidence that iron is in the +2 oxidation state, and a nonzerovalent oxidation state is also supported by the presence of ca. four oxygen neighbors for each iron atom. Incorporation of iron into the ZSM-5 framework may be ruled out by comparison to EXAFS results for iron incorporated into a silicalite framework.[9] As would be expected, spectra of these materials show no evidence at all of iron−iron interatomic distances.

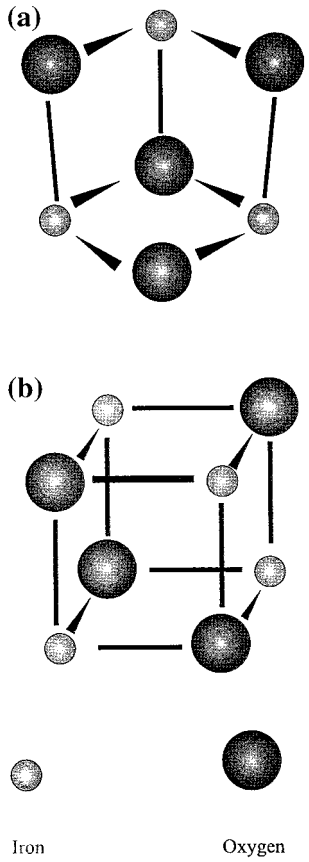

Figure 13. Possible structural analogues of the iron−oxo nanoclusters formed within the ZSM-5 pores: (a) ferredoxin (II); (b) HIPIP.

We therefore propose that these short iron−iron distances of ca. 2.5 Å occur in very small iron−oxygen clusters of unusual structure, the average iron−iron coordination number between 2 and 3, suggesting that these clusters contain three to four iron atoms. Because of their small size and their very high stability against reduction, we refer to them as *ultrastable nanoclusters*, and we have examined the literature for possible structural analogues. Unique iron−oxygen clusters have been made from the gas-phase oxidation of carbonyls[39] or laser-evaporated metal.[40,41] There are of course no structural studies of these materials, but the most detailed models for their geometry focus on clusters containing up to six iron atoms with a lone or single oxygen,[40] perhaps similar to the metal carbido clusters known in organometallic chemistry. The calculated Fe−O and Fe−Fe distances for the Fe_2O cluster, at 1.77 and 2.02 Å, respectively, are far smaller than the distances we find in our materials. In a preliminary report, we have therefore argued that the iron−oxygen clusters formed within the ZSM-5 zeolite are analogues of iron−sulfur clusters found in biological molecules such as the ferredoxins[42] or HIPIP (high-potential iron protein),[43] whose structures are shown in Figure 13.

Reduced ferredoxins exhibit an Fe−Fe distance of 2.67 Å, ca. 0.25 Å shorter than the smallest metal−metal distance in iron(II) sulfide of 2.92 Å. The Fe−Fe bond in the zeolite bound cluster is shorter than the metal−metal distance in the ferredoxin, since oxygen is a smaller atom than sulfur. In support of this, the nearest-neighbor Fe−O and FeS distances in FeO and FeS differ by about 0.2 Å. The oxygen ionic radius is as much as 0.4 Å smaller than that of S^{2-}, whereas we note a difference of only 0.2 Å, suggesting that the iron−oxo clusters have significant covalent character. Calculating an Fe−Fe distance in the zeolite oxo clusters from the structure of reduced HIPIP[21] yields a value of 2.50 Å, in excellent agreement with the

TABLE 6: Assignments of Infrared Bands Observed as a Result of NO Adsorption

frequency/cm^{-1}	assignment
1786	low-spin Fe(I)−NO^{+} complex
1816	second NO molecule on Fe−oxo nanocluster
1841	NO on isolated Fe^{2+}
1880	NO on Fe cluster
2135	NO^{+} on H^{+}

[a] For discussion see text.

experimental value of 2.51 ± 0.02 Å. We do not believe that the very short iron−iron interatomic distances or the observation of Fe−Fe coordination numbers greater than 1 is consistent with the structural proposal of FH, namely, the existence of [Fe^{2+}−O^{2-}−Fe^{2+}]$^{2+}$ species.[7,14] Where analogous species are known to occur, for example, in Cu−ZSM-5, the distances between the metal atoms are typically 2.9−3.0 Å, resembling those in the bulk oxide.[8]

4.3. Fe−ZSM-5 Activated in the Presence of Oxygen. As expected, catalysts activated in oxygen are initially in the +3 oxidation state, as indicated by the similarity of the near-edge structure to that of iron(III) oxide (Figure 8a), and EXAFS results show higher oxygen coordination numbers than observed under, for example, vacuum treatment (Figure 4b and Table 3). TPR of the oxygen- or air-treated materials also exhibited a small reduction feature at ca. 750 K, attributable to the partial reduction of Fe(III) species to Fe(II). Apart from these expected differences, the EXAFS results are very similar to those for the materials treated in a vacuum, which we have already discussed, again suggesting the presence of iron−oxo *nanoclusters*.

Two significant differences resulting from different pretreatment regimes, however, need to be considered: the effect on the observed Brønsted acidity and the effect on catalytic activity. Figure 13 shows that samples pretreated in an inert atmosphere show about twice the SCR activity of those exposed initially to oxygen. Moreover, this effect is irreversible, since it is not influenced by subsequent exposure to a different atmosphere. Figure 1 and Table 1 show that, while some 27% of the zeolitic protons are displaced after anaerobic treatment, there is little change as a result of activation in oxygen.

These differences suggest that these clusters contain at least two different iron-containing entities of different catalytic activity, which we propose to be the *ultrastable nanoclusters* already discussed and isolated iron ions. We will return to this point in considering the NO adsorption results in detail.

4.4. Adsorption Complexes and Reactions with NO. The adsorption of nitric oxide studied by infrared spectroscopy enables us to probe a number of different and important features of our iron/ZSM-5 materials and allows comparisons with other metal−zeolite catalysts. NO adsorption should also provide information on the *heterogeneity* of iron−oxo species within the zeolites, which averaging methods such as EXAFS cannot explore. In particular, we look to this approach to indicate the occurrence of *isolated* iron species, which are the majority entities in Cu−ZSM-5.[8]

NO interacts much more strongly with Fe(II) than with Fe(III),[46] so the main discussion concerns samples treated in inert atmospheres. The most important bands observed and the assignments that we propose are indicated in Table 6. Adsorption at 10^{-3} mbar, the lowest NO pressure used, results in bands at 1880 cm^{-1} with small peaks causing shoulders at 1841 and 1816 cm^{-1}. The exact positions of the minor peaks have been determined by peak fitting. The way in which the bands evolve as the NO pressure is increased has been described in section 3.4 and is shown in Figures 10 and 11. NO adsorption on Fe−ZSM-5 results in vibration frequencies considerably higher than observed on copper-exchanged metal zeolites, where the main bands are at 1812 and 1734 cm^{-1}. Frequencies are nearer to the gas-phase value for NO (1890 cm^{-1}), although desorption experiments clearly indicate an equally strong NO bond to the Fe clusters. The combination of markedly different vibration frequencies with comparable adsorption strength strongly implies the existence of different adsorption sites or geometry for NO on Fe−ZSM-5 compared to Cu−ZSM-5.[44]

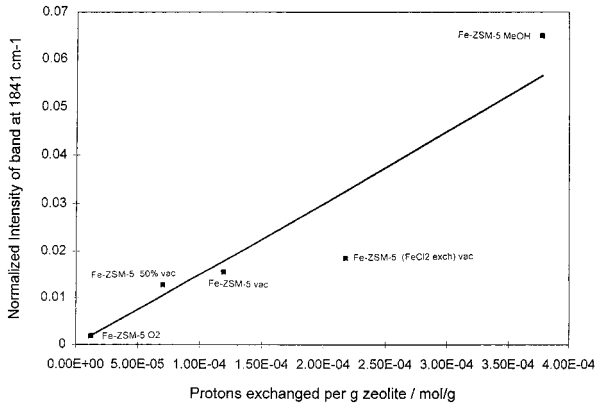

Figure 14. Relationship between the number of protons removed by the introduction of iron into ZSM-5 and the intensity of the band due to adsorbed NO at 1841 cm^{-1}. Spectra were recorded at 303 K and $P_{NO} = 10^{-3}$ mbar.

Some of the bands that we have found for NO adsorption on Fe−ZSM-5 have also been noted on iron/faujasite materials. Those at 1880, 1768, and 1816 cm^{-1} respectively have been attributed to a high-spin Fe(II)−NO complex, to a low-spin Fe(II)−NO complex[45] involving isolated Fe(II) ions, and to adsorption on more covalent Fe−O−Fe species.[46] In faujasite, it is believed that the low-spin and high-spin complexes are respectively located in the small and large cavities.[46] On the basis of a combination of Mössbauer spectroscopy, EPR, and infrared spectroscopy, it has been argued that the feature at 1816 cm^{-1} is due to species such as Fe^{2+}−O−Fe^{2+}.[1,45,46] Mössbauer isomer and quadrupole shifts have been observed in Fe−FAU that are comparable to those of iron(II) sulfide,[47] supporting the conclusions from our EXAFS results.

We draw attention to the existence of an important linear relationship between the intensity of the NO stretching vibration at 1841 cm^{-1} and the number of acid sites in the zeolite that are destroyed by the introduction of iron, as shown for five materials prepared in different ways in Figure 14. The reasonable linear relationship suggests that this band is due to adsorption only on *isolated* iron ions, since the number of NO molecules adsorbed is expected to vary with cluster size, leading to a nonlinear relationship if NO were adsorbed on the clusters. Formation of the *nanoclusters* thus does not result in marked displacement of Brønsted acidity from the ZSM-5. Figure 14 therefore suggests that almost no isolated ions occur on materials prepared by aqueous exchange and subsequent calcination in oxygen but that their number increases to a maximum for catalysts made by exchange from methanol solutions of Fe(III) nitrate. Where *isolated* species coexist with *nanoclusters*, the average cluster size will of course be somewhat larger than the value deduced from the Fe−Fe coordination number.

We believe that the band at 1880 cm^{-1} results from NO adsorption on the iron−oxo nanoclusters whose structure has been discussed above, since the normalized intensity of this band is highest on the sample prepared by aqueous exchange, heated

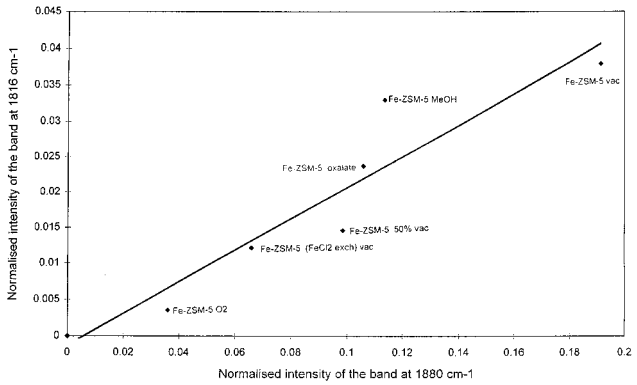

Figure 15. Relationship between the normalized intensities of bands at 1816 and 1880 cm^{-1} for four different samples in contact with 10^{-2} mbar NO.

in nitrogen (see Table 3), which also shows the highest coordination number for the Fe−Fe cluster distance at ca. 2.5 Å.

The band at 1816 cm^{-1} exhibits interesting dynamic behavior. Once the band at 1880 cm^{-1} reaches its final intensity, the band at 1816 cm^{-1} increases in intensity. One possibility is that the band at 1816 cm^{-1} is due to additional adsorption of NO on an Fe−NO complex. Thus, the band at 1816 cm^{-1} can be attributed to NO adsorbed either on clusters with preadsorbed NO or on a different structural unit. Figure 15 shows the relationship between the intensities of the bands at 1816 cm^{-1} and at 1880 cm^{-1} for different samples in contact with 10^{-2} mbar NO. A strictly linear relationship between these two bands would indicate that the resulting bands are due to adsorption on one structural unit. The relationship we found exhibits some deviations from linearity; however, we believe this is within the experimental error. Since the band at 1816 cm^{-1} only appears significantly when the band at 1880 cm^{-1} has reached its final intensity and increases further at higher NO pressures, band intensity determination is strongly dependent on exact pressures and temperatures over the different zeolite samples. Small deviations in the pressures and temperatures will lead to large deviations in band intensities and thus to higher uncertainties. However, the general trend clearly suggests a relationship, and thus, we believe that the band at 1816 cm^{-1} is due to adsorption on the cluster sites with preadsorbed NO. The band at 1786 cm^{-1} is believed to be due to a low-spin Fe(I)−NO^+ complex, as suggested by Lunsford et al.,[45] which can easily be formed from the high-spin complex by changing experimental conditions.

A broad feature at 1635 cm^{-1}, posssibly including several new bands, is observed when the system is evacuated following NO adsorption at 10 mbar. Samples activated in a vacuum exhibited bands after adsorption and subsequent evacuation that can be attributed to nitrite or nitrate species.[48−51] The presence of these species suggests the occurrence of disproportionation reactions such as

$$4NO \rightarrow N_2 + 2NO_2$$

possibly induced by multiple NO adsorption at a single cluster or ion. Some similar bands were observed following initial treatment of Fe−ZSM-5 in oxygen and exposure to NO (Figure 10a), although the concentration of adsorbed species was reduced presumably because of the relative inactivity of Fe(III) toward NO. With increasing NO pressure, a band at 2141 cm^{-1} increases in intensity. This band can be attributed to NO^{2+} species hydrogen-bonded to the acidic OH groups of the zeolite[50] or to NO^+ species acting as a charge-balancing cation.[52] These results indicate in either case that some adsorbed oxygen remains within the zeolite framework or that disproportionation reactions occur as indicated above, even after evacuation at 10^{-7} mbar, and that it is able to react with NO, either forming NO_2 or NO^+ and water. As mentioned in the structural discussion (section 4.2), the presence or absence of oxygen in the first activation step results in the formation of a different distribution of iron species. It is considered significant also that the number of Brønsted sites observed is determined by the initial calcination environment and is not modified by subsequent treatments.

4.5. Selective Catalytic Reduction of NO_x over Fe−ZSM-5. As shown in Figure 12, the Fe−ZSM-5 materials are active in the SCR reaction. Absolute activities are lower than for Cu−ZSM-5,[20] but because the iron loadings are also much lower, the highest turnover frequencies observed (in the range 3.5×10^{-3}/mol NO/(mol Fe s^{-1})) at 675 K are typically twice those of over-exchanged Cu−ZSM-5,[27] which has served as a benchmark catalyst for this reaction.

The most interesting feature of the catalytic results is the higher activity of samples initially pretreated in an inert atmosphere compared to those calcined in the presence of oxygen. Figure 12 shows that this difference is *irreversible*, since subsequent treatment of either material in oxygen or an inert atmosphere does not change their activity.

The catalytic activity of the different materials is also related to their NO adsorption capacity. Figure 16a shows that there is a clear relationship between NO adsorption and catalytic activity in the SCR reaction. The more NO that can be adsorbed, the higher the catalytic activity that is achieved. Figure 16b, which plots the results in a different way, shows that higher catalytic

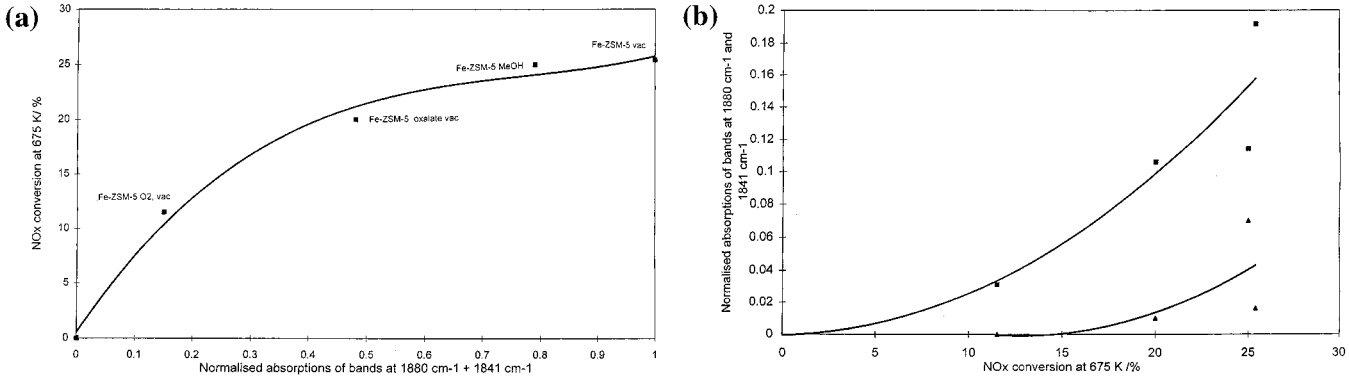

Figure 16. (a) Relationship between the activity in the SCR reaction at 775 K and the total NO adsorption capacity of different samples at 305 K and $P_{NO} = 10^{-3}$ mbar, determined by infrared spectroscopy. (b) Relationship between the intensities in the individual IR bands at 1880 cm^{-1} (diamond) and 1841 cm^{-1} (square) and NO_x conversion activity at 675 K. Note that substantial catalytic activity is observed before finite intensity is seen in the band at 1841 cm^{-1}.

activity is associated with the band at 1880 cm^{-1}, which we assign to adsorption on the oxo *nanoclusters*. Significant catalytic activity is observed even when the band at 1841 cm^{-1} is absent, suggesting that the isolated iron ions are of relatively low activity.

Comparison of the catalytic performance of the materials studied indicates that those with the higher proportion of nanoclusters are the most active, but those that contain predominantly isolated ions still show some activity. This shows that both the nanoclusters and the isolated iron ions possess catalytic activity but that each iron atom in a nanocluster is more active than if it were an isolated ion. Similar suggestions have recently been made by Sachtler et al.[53]

We have not carried out reactivity studies in the presence of water or sulfur dioxide and so are unable to comment on the reports of FH that some of these materials show unusual stability. Under our test conditions, the activity of catalysts prepared by the FH procedure is lower than those prepared by aqueous exchange but activated in an inert atmosphere. The activity of the samples prepared by exchange in methanol is similar to Fe−ZSM-5(vac).

4.6. Interaction of the Cluster with the Zeolite. The infrared and EXAFS results indicate the presence of two types of iron-containing species: mononuclear ions and oxo *nanoclusters*. Taken together, the EXAFS results, the NO adsorption studies, and the catalytic measurements all indicate that the distribution of these species and the way in which they interact with the zeolite are determined irreversibly by the preparation method and the pretreatment that the samples receive. Different preparations and pretreatments influence the relative concentration of these two types of species.

Figure 14 indicates that there is a linear relationship between the concentration of isolated cations and the number of protons removed in the exchange process. This is not easy to explain, since it is believed that a polyvalent cation will normally be able to interact with only one framework aluminum ion.[54] The linear relationship suggests that there is a nonrandom distribution of framework aluminum in these particular samples.

Determining the charge on the oxo clusters and the way in which they interact with the zeolite cannot be done with any certainty, and it should be remembered that little apparent exchange of protons is associated with cluster formation. A cluster of composition resembling ferredoxin, $Fe(III)_3O_4$, will have a formal charge of +1 and so might be expected easily to replace a proton. A cluster of composition $Fe(II)_4O_4$ would be neutral and need only be associated with an acidic proton by hydrogen bonding. At higher exchange levels we observe a broad band in the infrared spectrum at 2670 cm^{-1}, which could be associated with this type of nonclassical exchange. The situation is, however, complex, since our EXAFS results and microbalance studies by FH[14] both suggest that the redox chemistry of these materials involves a single electron-transfer per iron atom.

5. Conclusions

Exchange of iron into the zeolite ZSM-5 leads to the formation of both isolated iron atoms and iron−oxo nanoclusters of typical size Fe_4O_4 and with the very short iron−iron interatomic distance of ca. 2.50 Å. The distribution of species, which has been studied by both EXAFS spectroscopy and the use of NO as a probe molecule, varies with preparation method and, crucially, with the nature of the pretreatment. Pretreatment in an inert atmosphere leads to a higher concentration of the *nanoclusters* and to materials that are more active in the selective catalytic reduction of NO_x in the presence of excess oxygen (the SCR reaction). Pretreatment in oxygen leads irreversibly to a material with lower catalytic activity and a lower number of clusters. All of the iron species can undergo ready and reversible interconversion between Fe(II) and Fe(III), but in the presence of hydrogen reduction to the metallic state does not occur below 1250 K. The interaction of the iron species with the zeolite framework and with the acidic protons is complex and is not fully understood.

Acknowledgment. We are very grateful to Dr. C. J. Kiely and Mr. G. McPherson (Department of Materials Science and Engineering, University of Liverpool) for the electron microscopy study, to Ms. J. Connerton for performing the catalytic measurements and assisting in the X-ray absorption experiments, and to Drs. A. Dent (CCRL Daresbury Laboratory) and J. S. J. Hargreaves, who also assisted in the X-ray absorption experiments. We are also grateful to Professor W. Keith Hall for helpful discussions and access to a preprint. We gratefully acknowledge the financial support of this work by the Engineering and Physical Sciences Research Council.

References and Notes

(1) Morice, J. A.; Rees, L. V. A. *Trans Faraday Soc*. **1968**, *64*, 1388.
(2) Delgass, W. N.; Garten, R. L.; Boudart, M. *J. Catal*. **1970**, *18*, 90.
(3) Valyon, J.; Millman, W. S.; Hall, W. K. *Catal. Lett*. **1994**, *24*, 215.
(4) Sobolev, V. I.; Panov, P. I.; Kharitoniov, A. S.; Romannikov, V. N.; Volodin, A. M.; Ione, K. G. *J. Catal*. **1993**, *139*, 435.
(5) Panov, G. I.; Sobolev, V. I.; Dubkov, K. A.; Kharitonov, A. S. *Stud. Surf. Sci. Catal*. **1996**, *101*, 493. (a) Anderson, J. R.; Tsai, P. *J. Chem. Soc., Chem. Commun.* **1987**, 1435.
(6) Sato, S.; Hirabayashi, H.; Yahiro, H.; Mizuno, N.; Iwamoto, M. *Catal. Lett*. **1992**, *12*, 193.
(7) Feng, X.; Hall, W. K. *Catal Lett*. **1996**, *41*, 45.
(8) Grunert, W.; Hayes, N. W.; Joyner, R. W.; Shpiro, E. S.; Siddiqui, M. R.; Baeva, G. N. *J. Phys. Chem*. **1994**, 10832.
(9) Axon, S. A.; Fox, K. F.; Carr, S. W.; Klinowski. J. *Chem. Phys. Lett.* **1992**, *189* (1), 1.
(10) Lewis, D. W.; Catlow, C. R. A.; Sankar, G.; Carr, S. W. *J. Phys. Chem*. **1995**, *99*, 2377.
(11) Rey, F.; Sankar, G.; Maschmeyer, T.; Thomas, J. M.; Bell, R. G.; Greaves, G. N. *Top. Catal*. **1996**, *3*, 21.
(12) Bordiga, S.; Buzzoni, F.; Geobaldo, F.; Lamberti, C.; Giamello, E.; Zechina, A, Leofanti, G.; Petrini, G.; Tozzola, G.; Vlaic, G. *J. Catal*. **1996**, *158*, 486.
(13) Lazar, K.; Pal-Borbely, G.; Beyer, H. K.; Karge, H. G. *Stud. Surf. Sci. Catal*. **1994,** *91*, 551.
(14) Feng, X.; Hall, W. K. *J. Catal*. **1997**, *166*, 368.
(15) Hall, W. K.; Feng, X.; Dumesic, J.; Watwe, R. *Catal. Lett.* **1998**, *52*, 13.
(16) Davies, R.; Dent, A.; Joyner, R. W.; et al. In preparation.
(17) See, for example, the following. Joyner, R. W. In *Elementary Reaction Steps in Heterogeneous Catalysis*; Joyner, R. W., van Santen, R. A, Eds.; Kluwer: Dordrecht, 1993; p 249.
(18) Joyner, R. W.; Martin, K. J.; Meehan, P. *J. Phys. C* **1987**, *20*, 4005−4012.
(19) Schofield, J. H. *J. Electron Spectrosc. Relat. Phenom*. **1976**, *8*, 129.
(20) Connerton, J.; Joyner, R. W.; Stockenhuber, M. *J. Chem. Soc., Chem. Commun.* **1997**, *2*, 185.
(21) Jentys, A.; Lercher, J. A. *Stud. Surf. Sci. Catal 46*, 585.
(22) Fritz, P. O.; Lunsford, J. H. *J. Catal*. **1989**, *118*, 85.
(23) Aronson, M. T.; Gorte, R. J.; Farneth, W. E. *J. Catal*. **1987**, *105*, 455.
(24) Shpiro, E. S.; Grunert, W.; Joyner, R. W.; Baeva, G. N. *Catal. Lett*. **1994**, *24*, 159.
(25) Kaliaguine, S.; Adnot, A.; Lemay, G.; Rodrigo, L. *J. Catal*. **1989**, *118*, 275.
(26) Mahay, A.; Lemay, G.; Adnot, A.; Szoghy, I. M.; Kaliaguine, S. *J. Catal*. **1987**, *103*, 480.
(27) Connerton, J.; Joyner, R. W. *Stud. Surf. Sci. Catal*. **1998**, *116*, 327.
(28) Li, Y.; Armor, J. N. *Appl. Catal. B* **1992**, *1*, L21.
(29) Valyon, J.; Millman, W. S.; Hall, W. K. *Catal. Lett*. **1994**, *24*, 215.
(30) Inamura, K.; Iwamoto, R.; Iino, A.; Takyu, T. *J. Catal*. **1993**, *142*, 274.
(31) Koh, D. J.; Chung, J. S.; Kim, Y. G. *Catal. Lett*. **1995**, *33*, 57.
(32) Li, Y.; Battavio, P. J.; Armor, J. N. *J. Catal*. **1993**, *142*, 561.

(33) Cotton, F. A.; Wilkinson, G. *Advanced Inorganic Chemistry*, 5th ed.; John Wiley and Sons: New York, 1988.
(34) Greenwood, N. N.; Earnshaw, A. *Chemistry of the Elements*, 1st ed.; Permagon Press: Oxford, 1984; p 1265.
(35) Kanebo, K.; Kosugi, N.; Huroda, H. *J. Chem. Soc., Faraday Trans.* **1989**, *85* (4), 869.
(36) Joyner, R. W.; Stockenhuber, M. In *Abstracts of the 3rd European Congress on Catalysis*; Institute of Catalysis and Surface Chemistry, Polish Academy of Science: Krakow, 1997; Vol. 688 and this communication.
(37) Shirane, G.; Pickart, S. J.; Nathans, R.; Ishikawa, Y. *J. Phys. Chem. Solids* **1995**, *10*, 35.
(38) Kou, Y.; Sou, Z.; Wang, H. *J. Catal.* **1994**, *149*, 247.
(39) Jacobson, D. B.; Freiser, B. S. *J. Am. Chem. Soc.* **1986**, *108*, 27.
(40) Wang, L.; Fan, J.; Lou, L. *Surf. Rev. Lett.* **1996**, *3*, 695.
(41) Loh, S. K.; Lian, L.; Armentrout, P. B. *J. Chem. Phys.* **1989**, *91*, 6148.
(42) Kissinger, C. R.; Adman, E. T.; Sieker, L. C.; Jensen, L. H. *J. Am. Chem. Soc.* **1988**, *110*, 8721.
(43) Cramer, S. P. In *X-ray Adsorption, Principles, Applications, Techniques of EXAFS, SEXAFS and XANES*; Konigsberger, D. C., Prins, R., Eds.; Chemical Analysis 92; Wiley: New York, 1988 and references therein.
(44) Hayes, N. W.; Joyner, R. W.; Shpiro, E. S. *Appl. Catal. B* **1996**, *8*, 343.
(45) Jermyn, J. W.; Johnson, T. J.; Vansant, E. F.; Lunsford, J. H. *J. Phys. Chem.* **1973**, *77*, 2964.
(46) Davydoff, A. A. In *Infrared Spectroscopy of Adsorbed Species on the Surface of Transition Metal Oxides*; Wiley: New York, 1990.
(47) Morice, J. A.; Rees, L. V. C. *Trans. Faraday Soc.* **1968**, *64*, 1388.
(48) Hoost, T. E.; Laframboise, K. A.; Otto, K. *Appl. Catal. B* **1995**, *7*, 79.
(49) Kucherov, A. V.; Slinkin, A. A.; Kondreatev, A. A.; Rubinshtein, T. N.; Minachev, K. M. *Zeolites* **1985**, *5*, 320.
(50) Hoost, T. E.; Laframboise, K. A.; Otto, K. *Catal. Lett.* **1996**, *37*, 153.
(51) Aylor, A. W.; Larsen, S. C.; Reimer, J. A.; Bell, A. T. *J. Catal.* **1995**, *157*, 592.
(52) Hadjiivanov, K.; Saussey, J.; Freysz, J.; Lavalley, J. C. *Catal. Lett.* **1998**, *52*, 103.
(53) Voskoboinikov, T. V.; Chen, H.; Sachtler, W. M. H. *Appl. Catal. B* **1998**, *19*, 279.
(54) Feng, X. B.; Hall, W. K. *Catal. Lett.* **1997**, *46*, 11.
(55) Song, I.; Antonia, M. R.; Payer, J. H. *J. Electrochem. Soc.* **1995**, *142*, 2219.